District-scale numerical analysis of settlements related to groundwater lowering in variable soil conditions

Peduto, Dario; Prosperi, Alfonso; Nicodemo, Gianfranco; Korff, Mandy

DOI
10.1139/cgj-2021-0041

Publication date
2022

Document Version
Final published version

Published in
Canadian Geotechnical Journal

Citation (APA)
Peduto, D., Prosperi, A., Nicodemo, G., & Korff, M. (2022). District-scale numerical analysis of settlements related to groundwater lowering in variable soil conditions. *Canadian Geotechnical Journal*, *59*(6), 978-993. https://doi.org/10.1139/cgj-2021-0041

Canadian Science Publishing

ARTICLE

District-scale numerical analysis of settlements related to groundwater lowering in variable soil conditions

Dario Peduto, Alfonso Prosperi, Gianfranco Nicodemo, and Mandy Korff

Abstract: This study presents a novel framework in which numerical modelling contributes to the performance of district-scale, subsidence-induced damage assessment in cities where ground settlements affect entire quarters. Therein, the implementation of expeditious procedures offers geotechnical engineers the possibility of contributing beyond the typical site scale. For this purpose, several "typified" hydro-geomechanical-loading (HGL) models, which represent (simplified) scenarios of masonry buildings undergoing settlements, were set up to account for different predisposing or triggering factors (i.e., soil heterogeneity, loading conditions, and groundwater variations) of settlement occurrence in built-up areas. These models exploit multi-source, wide-area input datasets encompassing the hydro-mechanical properties of geomaterials, in situ investigations and measurements (e.g., groundwater levels in wells), and innovative remote sensing data (i.e., DInSAR techniques). With reference to a district in Rotterdam City (the Netherlands), which was built on "soft soils", the numerical simulations of different scenarios (*i*) provide an overview of the comparative role of predisposing or triggering factors on settlement occurrence and (*ii*) allow assessments of the expected induced damage to masonry buildings over 30 years with the exploitation of fragility curves. Considering the widespread diffusion of such geohazards, the proposed approach could help prioritise (rather expensive) maintenance work to the built heritage within sustainable strategies for subsidence risk mitigation.

Key words: settlement modelling, building damage assessment, soil variability, groundwater lowering, soft soils.

Résumé : Le but de la présente publication est de présenter un nouveau cadre au sein duquel la modélisation numérique contribue à la performance de l'évaluation des dommages induits par les affaissements à l'échelle du quartier dans les villes où les tassements du sol affectent des quartiers entiers. La mise en œuvre de procédures rapides offre ainsi aux ingénieurs géotechniques la possibilité de contribuer à une évaluation au-delà de l'échelle typique du site. Dans ce but, différents modèles hydro-géomécaniques de chargement (HGL) « typés », permettant de représenter des scénarios (simplifiés) de bâtiments en maçonnerie subissant des tassements, ont été mis en place pour tenir compte des différents facteurs prédisposants ou déclencheurs (c'est-à-dire l'hétérogénéité du sol, les conditions de chargement et les variations des eaux souterraines) de l'apparition des tassements dans les zones bâties. Ce sont principalement les propriétés hydro-mécaniques des géomatériaux, les enquêtes et les mesures in situ (par exemple, le niveau des eaux souterraines dans les puits) et les données de télédétection innovantes (par exemple, les techniques DInSAR) qui sont exploitées dans ces modèles. Les simulations numériques de différents scénarios, en se référant à un quartier de la ville de Rotterdam (Pays-Bas), construit sur des « sols mous », (*i*) fournissent une vue d'ensemble du rôle comparatif des facteurs prédisposants ou déclencheurs sur l'apparition des tassements et (*ii*) permettent d'évaluer les dommages induits attendus sur les bâtiments en maçonnerie sur 30 ans grâce à l'exploitation des courbes de fragilité. Dans le cadre d'une stratégie durable d'atténuation des risques d'affaissement, la démarche suggérée permet de hiérarchiser les travaux d'entretien (plutôt coûteux) du patrimoine bâti, compte tenu de la diffusion généralisée de ces géorisques. [Traduit par la Rédaction]

Mots-clés : modélisation du tassement, évaluation des dommages aux bâtiments, variabilité du sol, abaissement de la nappe phréatique, sols mous.

1. Introduction

Many urbanised areas worldwide have subsided due to the presence of highly compressible soils (namely "soft soils"; Erkens et al. 2015; Herrera-García et al. 2021). The occurrence, magnitude, and distribution of ground settlements are highly influenced by soil variability (Breysse et al. 2005; Elkateb et al. 2003; Marache et al. 2009; Popescu et al. 2005), as well as by the groundwater regime (Guzy and Malinowska 2020; Mas-Pla et al. 2013; Modoni et al. 2013; Shahriar et al. 2013). This is the case in many delta countries such as the Netherlands, in which shallow subsurface layers consist of fluvial and coastal lowlands of the Holocene age comprising recent unconsolidated sedimentary deposits (Dufour 2000; van der Meulen et al. 2013). Such geological contexts expose

Received 31 January 2021. Accepted 24 September 2021.

D. Peduto and G. Nicodemo. Department of Civil Engineering, University of Salerno, via Giovanni Paolo II, 132, Fisciano, SA 84084, Italy.
A. Prosperi. Department of Civil Engineering, University of Salerno, via Giovanni Paolo II, 132, Fisciano, SA 84084, Italy; Faculty of Civil Engineering and Geosciences, Delft University of Technology, Stevinweg 1, Delft 2628 CN Delft/2600 GA, the Netherlands.
M. Korff. Faculty of Civil Engineering and Geosciences, Delft University of Technology, Stevinweg 1, Delft 2628 CN Delft/2600 GA, the Netherlands; Deltares, P.O. BOX 177, Delft P.O BOX 177, the Netherlands.

Corresponding author: Gianfranco Nicodemo (email: gnicodemo@unisa.it).

structures and infrastructure networks to settlement-induced damage. In the Netherlands, efforts have been made to predict the economic losses induced by subsidence-related damage to buildings; these forecasts range from 5 to 45 billion euros by 2050 (Bucx et al. 2015; Hoogvliet et al. 2012; Leusink 2018; van den Born et al. 2016). Consequently, subsidence risk is a topic of particular concern for both the scientific and technical communities when the most suitable strategies for land-use planning and urban management need to be identified.

To predict and prevent land subsidence effects, existing methods use regression models (Abdollahi et al. 2019; Lee and Park 2013) or hydro-mechanically coupled numerical simulations that consider both seepage and consolidation (Mahmoudpour et al. 2016; Shen and Xu 2011). However, these approaches generally require accurate spatially distributed datasets of subsoil features and hydro-geomechanical soil parameters. Furthermore, in urban areas, the transmitted loads of structures resting on the subsoil as well as possible variations in the pore pressure regimen induced by, for instance, the groundwater table drawdown due to anthropogenic activities (e.g., water withdrawal for civil or industrial use) need to be accounted for (Guzy and Malinowska 2020).

The above-mentioned aspects indicate that subsidence prediction is generally a difficult task because the results arise from a complex interplay among subsoil, superstructure, and foundation system (Ferlisi et al. 2020). This complex interaction problem is often handled by assuming that the subsoil system is composed of spatially homogeneous layers, thus ignoring the effects of soil heterogeneity (Frantziskonis and Breysse 2003).

Likewise, the monitoring of the subsidence-induced settlements affecting urbanised areas plays an essential role in structure–infrastructure performance control (Piciullo et al. 2021; Peduto et al. 2018, 2017*b*). Indeed, the collection of all the above information can be challenging when the analysis focuses on a single structure but is far more demanding when the study deals with a larger area (e.g., neighbourhood, city, region, or country). For instance, conventional monitoring techniques, such as levelling and GPS, can be unaffordable when the area of interest includes a large number of (infra) structures. This produces, in current engineering practice, patchy and discontinuous (over time) information whose assimilation in geotechnical settlement forecasting models can be challenging over wide areas (Peduto et al. 2017*a*).

Currently, a valuable contribution to these studies comes from national–regional datasets that are available to engineers. Among these, 2D–3D subsoil models (e.g., soil properties and stratigraphy) at the national/regional scale (e.g., the GeoTOP model in the Netherlands, www.dinoloket.nl; and the GeoEra 3DGEO-EU project for Europe, https://geoera.eu/projects/3dgeo-eu/), groundwater measurements (e.g., the REGIS II in the Netherlands, https://www.dinoloket.nl; the EPA HydroNet in Ireland, https://www.epa.ie/hydronet/; and the National Water Information System in the USA, https://waterdata.usgs.gov), and remote sensing techniques such as images acquired by spaceborne synthetic aperture radar (SAR) and processed via differential interferometric techniques (DInSAR) providing settlement measurements nationwide (Bischoff et al. 2020; Chang et al. 2017) on the regional–urban scale (Rosi et al. 2016) are worth mentioning. In particular, DInSAR represents a well-established noninvasive tool with submillimetre precision (Hanssen 2003) or accuracy (Peduto et al. 2018, 2019; Nicodemo et al. 2017) on the average velocity and subcentimetre accuracy of the single displacement (Herrera et al. 2009) on structures (Arangio et al. 2014; Peduto et al. 2017*b*; Pratesi et al. 2015) and infrastructure (Ferlisi et al. 2021; Giardina et al. 2019). More recently, this technique has been used in empirical approaches to assess the vulnerability of buildings (Fernández-Torres et al. 2020; Nicodemo et al. 2020*b*, 2020*c*; Peduto et al. 2019; Raspini et al. 2016) and road assets (Ferlisi et al. 2021; Nappo et al. 2019) undergoing settlements. Only a few case studies in the literature present the assimilation of these data in geotechnical modelling (Ezquerro et al. 2017; Modoni et al. 2013; Peduto et al. 2017*a*, 2020).

The analysis of data from monitoring techniques jointly with the settlements computed via numerical models can help to predict the damage occurrence in urban areas (Nicodemo et al. 2020*a*; Wu et al. 2020*a*, 2020*b*), using classical or innovative state-of-the-art tools for damage assessment. In geotechnical engineering practice, damage assessment is generally carried out using widely adopted empirical relationships based on the displacements experienced by foundations (Bjerrum 1963; Boscardin and Cording 1989; Burland and Wroth 1974; Polshin and Tokar 1957; Skempton and MacDonald 1956). In all encountered cases, the building damage assessment calls for a combination of threshold values of subsidence-related intensity parameters (SRI; Peduto et al. 2019), such as differential settlements, angular distortions, relative rotations, and deflection ratios, with different severity levels qualitatively distinguished by word classifications (e.g., from negligible to very severe; Burland et al. 1977).

When dealing with the assessment and prediction of damage to a large number of buildings, probabilistic (analytical, numerical or empirical, according to the input data source) fragility curves represent promising tools that relate different SRI parameter values to damage severity levels (Ferlisi et al. 2020; Peduto et al. 2019; Saeidi et al. 2012; Zhang and Ng 2005).

From the perspective of subsidence risk mitigation procedures, the present study aims to provide an original contribution to cities in which ground settlements affect entire districts. For this purpose, by combining multi-source information, a novel procedure developed at the district scale is proposed and applied within an urban area of the Netherlands. First, information about the spatial heterogeneity of the subsoil, typical loading (transferred by buildings) conditions, and water table drawdown measurements were collected from available wide-area datasets and analysed. This allowed the identification of 225 typical hydro-geomechanical-loading (HGL) models, resulting from combinations of the most common scenarios in the selected study area. Then, the defined HGL models were employed in numerical analyses to identify the "most critical" scenarios in terms of settlement occurrences and differential settlements affecting the buildings. At the same time, the roles played by the main predisposing or triggering factor(s) in the occurrence, magnitude, and spatial distribution of settlements in the study area were investigated. Finally, the outcomes of the numerical simulations (i.e., the differential settlements corresponding to the sample-building footprint) were implemented within the empirical fragility curves available for masonry buildings in the study area to forecast the structural damage throughout the analysed district.

2. Methodology

The procedure followed for the analyses consists of two main phases preceded by preliminary data collection (Fig. 1). In particular, the required basic input data, collected over the area of interest in the preliminary phase (Fig. 1), included (*i*) hydro-geomechanical properties of the recurrent soil layers along with their stratigraphic assets, (*ii*) groundwater-level measurements, and (*iii*) building features (e.g., structural typology, geometry, foundation type and mechanical properties of constituent materials).

The above data were used in Phase I (Fig. 1) to identify "typified" HGL scenarios. To this end, the input datasets were homogenised and examined at the district scale. First, the thicknesses of the soil types extracted from the investigated boreholes were analysed. In particular, the mean and standard deviation values of the cumulative soil thickness of the examined subsoil (i.e., peat, clay, silt, and sand) were obtained. Then, considering that the ground displacements associated with the presence of "soft soil" layers can be highly variable depending on their spatial distribution and cumulative thickness as well as their compressibility

Fig. 1. Flowchart of the adopted procedure. [Colour online.]

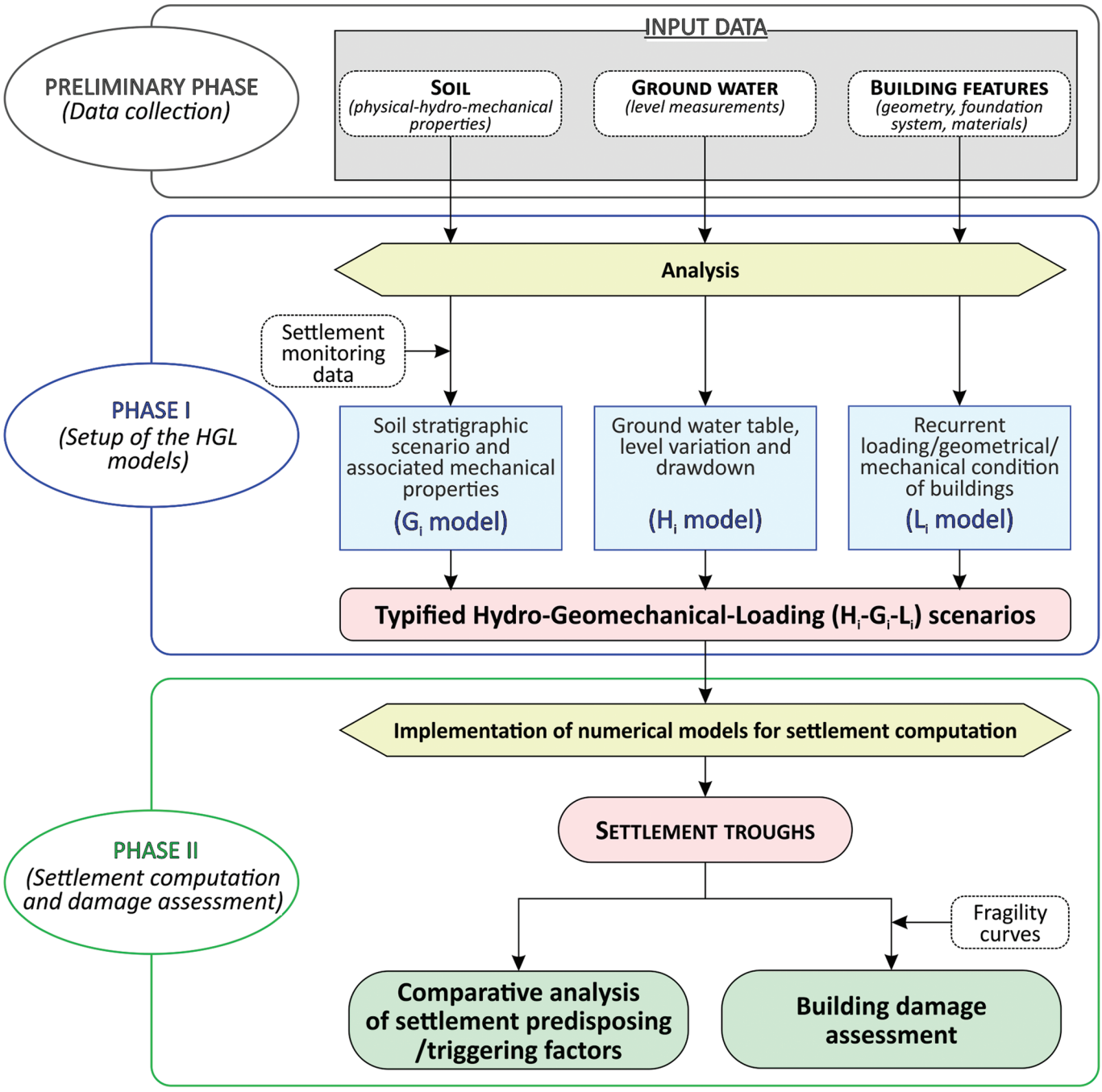

(Peduto et al. 2017*b*), geological cross-sections were drawn across the boreholes to derive typified subsoil stratigraphy and investigate the role played by the stratigraphic asset. Thus, the relationship between the "soft soil" (i.e., peat and clay) cumulative thickness along selected sections across the boreholes and the settlement magnitude under free-field conditions was investigated. For this purpose, in addition to the base input data collected during the preliminary phase, settlement monitoring data from innovative DInSAR techniques were used. In particular, DInSAR-derived settlements on the ground (i.e., in free-field conditions) were interpolated using the inverse distance weighted (IDW) method and compared with the cumulative thickness of "soft soil" extracted by the boreholes. Likewise, the DInSAR-derived cumulative settlements (years 2009–2014) measured on top of the buildings were compared with the settlements computed for built locations by means of simplified mono-dimensional numerical analyses conducted for each borehole considering the loads transferred by the buildings. In this step, the soft soil creep model (SSC) was assigned to peat, clay, and silt soils; a Mohr–Coulomb (MC) criterion was assigned to sand, and plastic calculations were carried out with a constant groundwater level.

The comparison between the computed mono-dimensional settlements and the measured settlements for each borehole allowed us to fix the soil mechanical parameters used in the following

analyses. In particular, the stratigraphical assets and the chosen mechanical parameters are jointly referred as geomechanical (G_i) conditions.

The groundwater level (and its variation) as well as the drawdown models (hereinafter referred to as the H_i model) were set up based on the analysis of time series data acquired from the available piezometric wells. Together with the observed water-head variation, this allowed for the definition of the time-dependent lowering functions used in the numerical simulations. The typical loading conditions (L_i) were established considering a model structure with its own weight, which was varied to represent the most common building geometries and, in turn, loading conditions in the district area.

Then, each geomechanical asset (G_i) was combined with all loading conditions (L_i), and for each geomechanical-loading condition (G_iL_i), all the drawdown models were applied, thus resulting in typified $H_iG_iL_i$ scenarios that were used for numerical simulations at the building scale in Phase II. In particular, finite element analyses were carried out for each defined HGL scenario by combining the geometry of the loading conditions (L_i), the stratigraphic assets and the physical–hydro-mechanical properties of the soil types (G_i), and the groundwater level (H_i) considering the lowering of the water table as the triggering factor for settlement occurrence. At this stage, numerical simulations were conducted by simultaneously considering the full interaction among deformations, consolidation, and groundwater flow. For this purpose, fully coupled flow-deformation analyses were carried out for the consolidation process, using the same constitutive law assigned in the numerical analyses of the mono-dimensional behaviour in correspondence of the boreholes (i.e., the SSC model was assigned to peat, clay, and silt soils, and an MC criterion was assigned to sand).

The results of the numerical simulation in terms of settlement troughs and associated differential settlements recorded in correspondence of the building footprint were then used to assess the role played by the different factors (i.e., stratigraphy, water drawdown, and loading conditions) contributing to building settlements. Empirical fragility curves available for the study area (Peduto et al. 2019) allowed the identification of the HGL scenarios exhibiting the highest probability of occurrence of the most severe damage levels corresponding to values of the SRI parameter (i.e., differential settlement) derived from the numerical analyses. Finally, these latter outcomes were used to predict the expected damage to the built heritage (buildings on shallow foundations) over the time considered for the numerical simulation.

3. Case study and available datasets

The urban area selected for the analysis was Bloemhof, a densely urbanised neighbourhood of Rotterdam City, located in the south-western part of the Netherlands (Fig. 2*a*), in an area belonging to the Rhine–Meuse Delta system. Rotterdam City rests entirely on upper Holocene clayey, peaty, and sandy (fine and middle categories in Fig. 2*b*) layers, which reach depths of approximately 20 m, overlapped with a Pleistocene layer of fine to coarse sands (coarse category in Fig. 2*b*) (De Doelder and Hannink 2015). The subsoil information used in this study was derived from the "GeoTOP model" (www.dinoloket.nl). The model, which extends down to a depth of 50 m below the ground surface, discretises the Dutch national territory in millions of voxels, each measuring 100 m × 100 m × 0.5 m (height × width × depth). Each voxel contains information on lithostratigraphy and lithological classes (including the probability of occurrence of each class) resulting from a systematic collection and subsequent geostatistical analysis of hundreds of thousands of borehole data and cone penetration tests (Stafleu et al. 2011). The physical–mechanical properties of soils were assumed to be those provided by the Dutch standards (NEN 9997-1+C2 2017) and are summarized in Table 1.

Bloemhof (Fig. 2*a*) is one of the most densely populated districts in the city. The neighbourhood was developed in the 1920s in an area characterised by the presence of soft soils and has been affected by subsidence (Hooimeijer et al. 2017). The built-up area presents different construction typologies (Fig. 2*c*), mostly consisting of 2–3 floored masonry buildings (typical row houses) resting on both shallow and deep foundations (Fig. 2*d*). Ghodsvali (2018) reported a few cases of buildings that recorded damage or even collapsed in the area due to the combined effect of subsidence and poor costruction quality (Fig. 2*e*).

Groundwater measurements and water-head levels acquired monthly (Gemeente Rotterdam 2020) in Rotterdam City are freely available from a monitoring network composed of approximately 2000 wells (30 of which are still operative and were chosen for the analyses over the study area; Fig. 3*a*). These measurements indicate that the groundwater level has been decreasing (an example for well W22 is shown in Fig. 3*b*). In this regard, Koster et al. (2018) presented a forecast analysis of subsidence potential in the Rotterdam municipality over a period of 15 and 30 years due to a groundwater decrease ranging from 0.1 to 0.4 m.

Over the study area, satellite DInSAR data, provided by SkyGeo, derived from the processing of 285 images acquired from 2009 to 2014 by the TerraSAR-X (TSX) satellite constellation on both ascending and descending orbits are available. The data consist of displacement measures at both the ground (e.g., free-field condition; Fig. 3*c*) level and on top of the building (at the roof level; Fig. 3*d*). These maps show that free-field displacement rates exceed 5 mm/year in many portions of the analysed district, whereas velocity values recorded on top of the buildings are rarely higher than 3 mm/year. Interestingly, as expected, by comparing Figs. 2*d* and 3*d* the highest settlement rates (Fig. 3*d*) seem to be concentrated in areas where buildings with shallow foundations prevail. Conversely, in the northernmost portion where buildings mainly rest on piled foundations, which may have acted as settlement-reducers (de Sanctis and Mandolini 2006; Randolph 1994; Russo and Viggiani 1998), settlement rates are below 1.5 mm/year (i.e., the accuracy of DInSAR data in similar contexts; Peduto et al. 2018) and thus are considered to be rather stable.

Finally, empirical fragility curves are available. These curves, derived ad hoc for 180 settlement-affected Dutch masonry buildings on shallow foundations (Peduto et al. 2019), provide probabilistic relationships between multiple SRI parameters and damage severity levels. The available fragility curves were used for the damage assessment and forecasting at the district scale.

4. Results

4.1. Preliminary phase

The necessary input data were collected for the study area according to the proposed procedure (Fig. 1). As for the stratigraphic assets of the recurrent soil layers and their physical–mechanical properties, the former were derived from 13 boreholes that were extracted from the GeoTOP model (Fig. 4*a*); the latter were assumed to be those provided by the Dutch standards (NEN 9997-1+C2 2017; Table 1).

The piezometric measurements (Fig. 3*a*), acquired from 1950 to 2020, were interpolated over the study area (Fig. 4*b*) using the IDW method on a 100 m × 100 m cell size (in agreement with the resolution of the GeoTOP model).

The buildings in Bloemhof belong to the typical row houses of the local architecture dating back to the 1920s (see, for instance, Fig. 2*e*). These buildings present similar volumes and ages and the same construction techniques, materials, and number of stories, according to the information retrieved by the Addresses and Buildings key register (Esri Nederland – BAG 3D 2020). In particular, the analysis presented hereafter focused on those buildings resting on shallow foundations that seem to exhibit the highest settlements as shown in Fig. 3*d*. The properties of the masonry walls were selected

Fig. 2. Study area: (*a*) cumulative thickness of soft soils (organic and clayey) in the Rotterdam area with (*b*) geological cross-section along the A–A′ profile sketched in panel (*a*) and zoomed along the Bloemhof district (extracted from the portal of the Geological Survey of the Netherlands — DINOloket, www.dinoloket.nl); maps of (*c*) building typologies (Esri Nederland – BAG 3D 2020) and (*d*) expected foundation types (Funderingskaart 2019) in Bloemhof district; (*e*) some photos of cracks on building façades. [Colour online.]

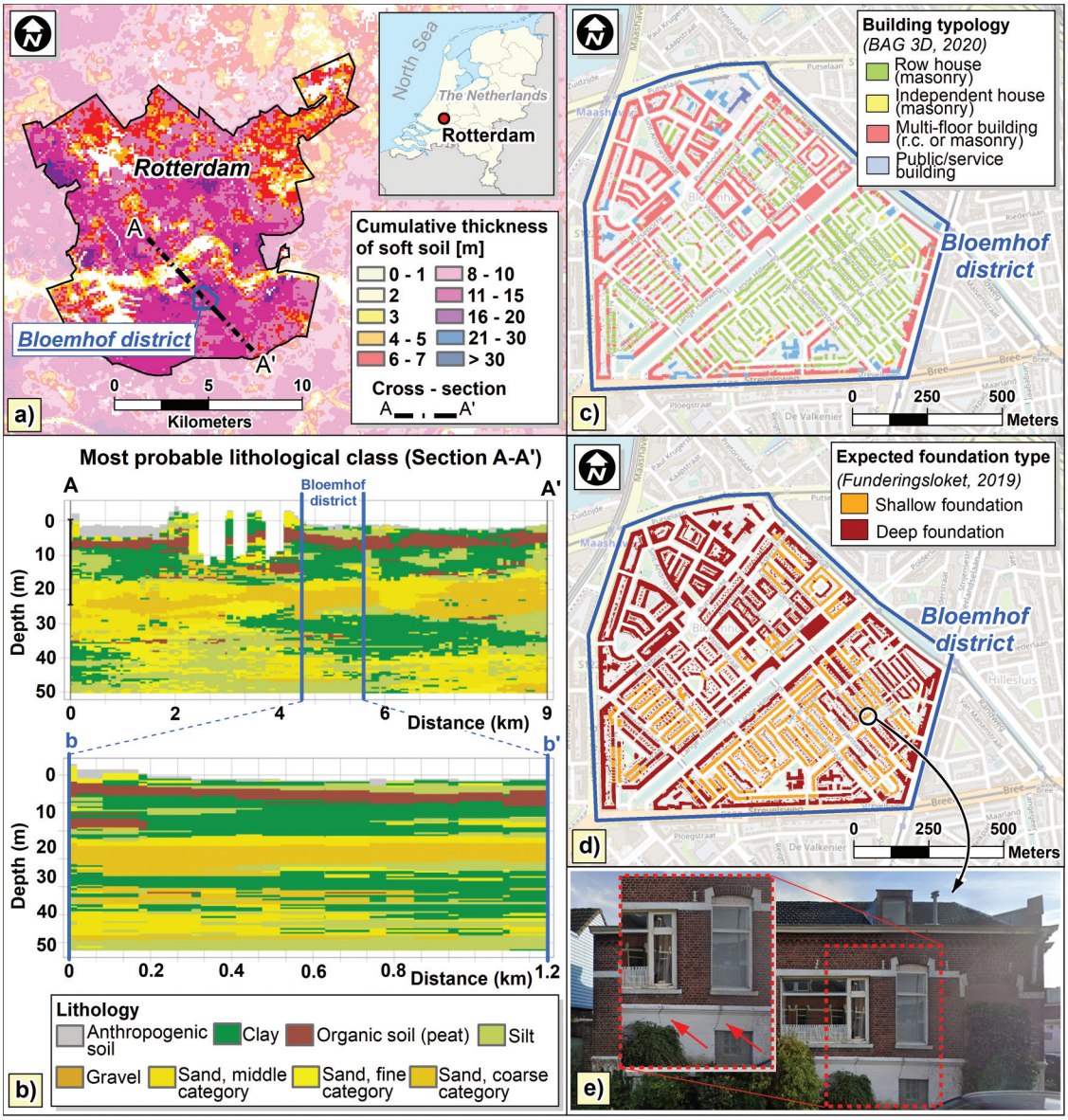

Table 1. Physical and mechanical properties of soil types in the study area.

	Physical and mechanical parameters											
Soil type	γ (kN/m^3)	γ_{sat} (kN/m^3)	$C_c/(1+e_0)$	E' (MPa)	ϕ'(°)	c' (kPa)	c_u (kPa)	k (m/s)	λ^*	k^*	μ^*	OCR
Anthropogenic soil	18.00	20.00	0.0038	45.0	32.5	0.0	—	1.16×10^{-5}	—	—	—	1.00
Holocene sand	18.00	20.00	0.0038	45.0	32.5	0.0	—	1.16×10^{-5}	—	—	—	1.00
Pleistocene sand	19.00	21.00	0.0023	75.0	35.0	0.0	—	1.16×10^{-5}	—	—	—	1.00
Silt	20.00	20.00	0.092	5.00	27.5	1.0	10	1.08×10^{-7}	0.0400	0.0080	0.0016	1.90
Clay	17.00	17.00	0.1533	2.00	17.5	5.0	50	3.41×10^{-10}	0.0667	0.0133	0.0027	1.90
Organic soil (peat)	12.00	13.00	0.3067	0.50	15.0	15.0	2.5	1.77×10^{-7}	0.1333	0.0267	0.0053	1.90

Note: γ, unsaturated unit weight; γ_{sat}, saturated unit weight; $C_c/(1+e_0)$, compression ratio; E', effective Young's modulus; ϕ', friction angle; c', effective cohesion; c_u, undrained shear strength; k, hydraulic conductivity; λ^*, modified compression index; k^*, modified swelling index; μ^*, modified creep index; OCR, over-consolidation ratio (from Dutch standards, NEN 9997-1+C2 2017).

Fig. 3. Groundwater measurements and available DInSAR dataset in the study area: (*a*) map of the water wells in the study area (Gemeente Rotterdam 2020); (*b*) example of the time series of water well level (from the portal Funderingskaart 2019); TSX DInSAR data on ascending and descending orbit at the ground level (*c*) and on the top of buildings (*d*). [Colour online.]

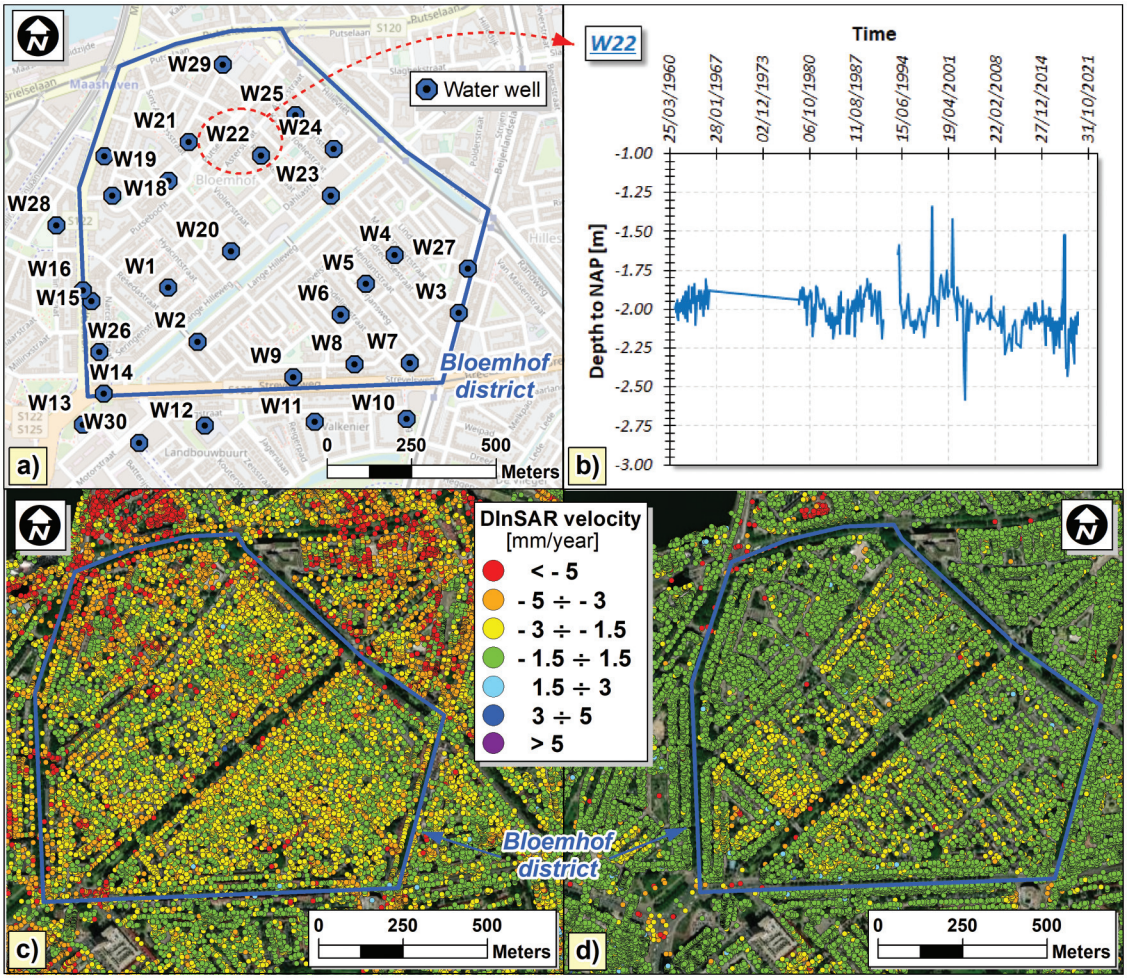

based on the NPR 9998 (2020) clay brickwork (pre-1945) values (Young's modulus E_m = 3000.00 N/mm^2, shear modulus G_m = 1200.00 N/mm^2, and an average unit weight of 18.00 kN/m^3).

4.2. Phase I: setup of the HGL models

The analysis of data gathered in the preliminary phase allowed us to define the equivalent geotechnical and loading models representing the "typified" HGL scenarios (Fig. 1). For this purpose, starting from the stratigraphy of the 13 selected boreholes (Fig. 4*a*), the mean and standard deviation of thickness values of peaty, clayey, silty, and sandy soil layers were calculated (Table 2).

To analyse the spatial variability of soft soil layers, the relationship between the "soft soil" (peat and clay) cumulative thickness and the DInSAR-derived cumulative settlement magnitude in free-field conditions was investigated. In particular, the vertical DInSAR-derived settlements at the ground level were computed by multiplying the average velocity of each coherent DInSAR benchmark (Fig. 3*c*) for the observation period (2009–2014). Then, DInSAR-derived cumulative settlements recorded at ground level were interpolated using the IDW method on a grid with a cell size of 100 m × 100 m (in agreement with the resolution of the GeoTOP model) over the study area, thereby generating the cumulative settlement map during the observation period (Fig. 5*a*). Interestingly, looking at the sample section across the B6–B7 boreholes (Fig. 5*b*), it can be observed that the soft soil (i.e., peat and clay), silt, and sand thickness did not show significant variations along the selected profile; nevertheless, a variation in the cumulative settlement profile is observable in borehole B6. Indeed, the highest recorded settlements at the ground level can depend on (*i*) the mutual thickness values (e.g., in borehole B6 there is an increase in peat and a decrease in clay thickness) along the section and (*ii*) the depth of a soil layer in a given location (e.g., shallower organic soil layers can be more influenced by a possible drawdown of the water table, leading to higher settlements). This is the case for borehole B6 where most of the peat is concentrated within a 5 m depth and a localised inclusion of organic material (this can lead to abrupt higher gradients of soft soil layer thickness along a cross section or even under the building foundation that, consequently, can be prone to differential settlements).

Accordingly, the thickness and slope of the soil layers under the loading area (building footprint) as well as organic soil inclusions were considered in the definition of the most common geostratigraphic (G_i) scenarios present in the study area.

As for the assigned physical–mechanical soil parameters (see Table 1), an expeditious validation test compared DInSAR-measured settlements on top of the buildings (derived by multiplying the average velocity of each coherent DInSAR benchmark (Fig. 3*d*) for the observation period 2009–2014) with the settlements computed

Fig. 4. (*a*) Position of the 13 considered boreholes (B*i*) in Bloemhof with the most probable lithoclass retrieved along the first 20 m of depth (from the portal of the Geological Survey of the Netherlands — DINOloket, www.dinoloket.nl); (*b*) spatial variation in the phreatic water table in Bloemhof derived from the interpolation of piezometric measurements in the period 1950–2020 (from the portal gis.rotterdam.nl) via the inverse distance weighted (IDW) method. [Colour online.]

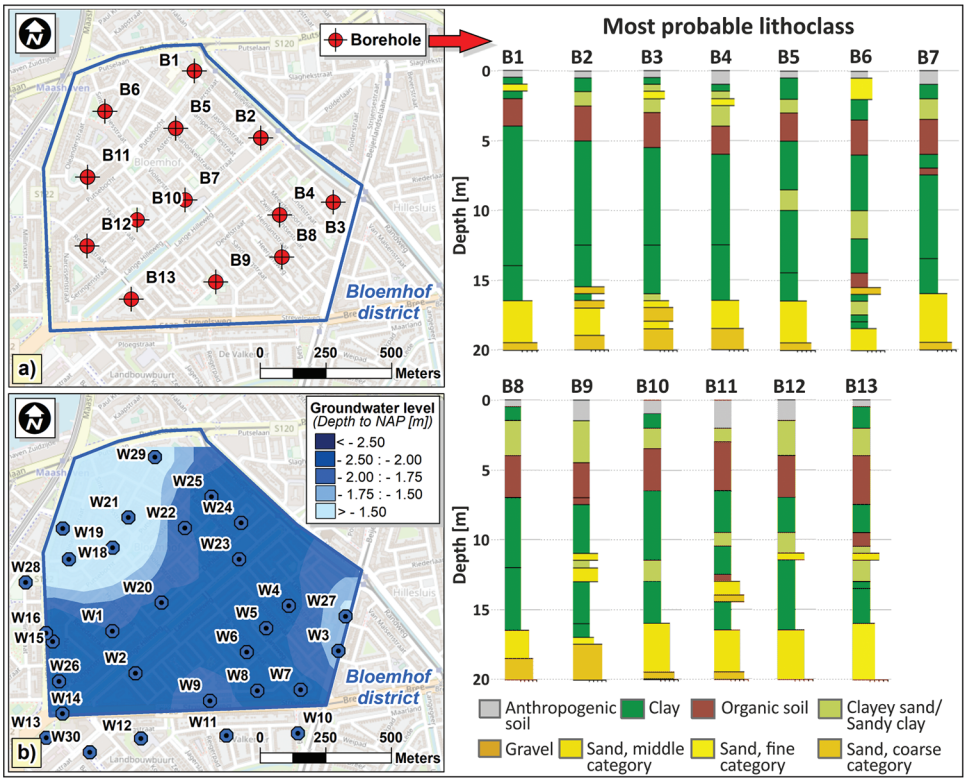

Table 2. Mean and standard deviation of soil layer thickness of the analyzed boreholes.

							Sand					
	Peat		Clay		Silt		Holocene		Pleistocene		Anthropogenic	
Depth range (m)	Mean (m)	SD (m)	Mean (m)	SD (m)	Mean (m)	SD (m)	Mean (m)	SD (m)	Mean (m)	SD (m)	Mean (m)	SD (m)
0–5	1.50	0.71	0.85	0.59	1.46	0.88	0.19	0.43	0.00	0.00	1.00	0.58
5–10	1.42	1.06	3.35	1.05	0.23	0.48	0.00	0.00	0.00	0.00	0.00	0.00
10–15	0.08	0.19	3.92	1.30	0.62	0.79	0.38	0.74	0.00	0.00	0.00	0.00
15–20	0.08	0.28	1.23	0.44	0.12	0.30	0.00	0.00	3.58	0.73	0.00	0.00

via simplified mono-dimensional analyses for each investigated borehole (Fig. 4*a*), also considering the building loads. The simulations were carried out with Plaxis2D software with a 5 year time interval, which is equal to the measurement period of DInSAR-derived cumulative settlements (years 2009–2014). Furthermore, starting from the map of the water table levels in the study area (Fig. 4*b*), wherein the groundwater level ranges between –2.50 and –1.50 m from the NAP (Normaal Amsterdams Peil) level, an average level equal to –1.50 m from the ground surface — obtained as the difference between the mean water table level (–2.00 m) and the average distance of the district surface level compared to the NAP level (–0.50 m) — was assumed. In this computation, a two-storey masonry building (with an average masonry wall weight of 18.00 kN/m^3) with wooden floors and a mat foundation system, whose footprint was equal to 200 m^2 (resulting in a mean load equal to 25.5 kN/m^2), was assumed. The results of numerical simulations (δ_c equal to Plaxis-2D computed settlement in Fig. 6) were then compared with DInSAR-measured (δ_m) cumulative settlements on top of buildings considering the coherent DInSAR benchmarks falling within a circular buffer of 100 m around each borehole (Fig. 6*a*). Thus, it was possible to determine that δ_m (reported with their mean and standard deviation in Fig. 6*b*) and δ_c (Fig. 6*b*) settlements exhibit satisfactory matching. Indeed, the δ_c values in 10 out of 13 cases fell within the confidence interval of δ_m during the observation period (i.e., 5 years). Interestingly, the values of Δ, computed as ($\delta_m - \delta_c$), never exceeded 5 mm in 5 years, thus falling within the accuracy of DInSAR data (1.5 mm/year) as shown by Peduto et al. (2019) for similar applications in the Netherlands. Thus, the mechanical properties of the geotechnical model derived from NEN 9997-1+C2 (2017; Table 1) were assumed to be suitable for subsequent analyses. As for the geomechanical (G_i) scenarios, five stratigraphic conditions were defined based on previous observations (i.e., the mean and standard deviations of soil thickness values; Fig. 7). To this end, two conditions pertaining to "nearby boreholes" (Fig. 7*a*) and "distant boreholes" (Figs. 7*b*) were considered in Plaxis2D. In particular, assuming a building with a façade length equal to "*d*" that rests on a given soil scenario, a nearby boreholes condition (Fig. 7*a*) represents the typical situation in which a "rapid" change in the soil layer (thickness and inclination) can occur between two fixed boreholes located at a distance not greater than *d* from the middle vertical line of the building; this means that the two assumed boreholes are at a maximum distance of 2*d* from each other (Fig. 7*a*). Conversely, the distant

Fig. 5. Analysis of the stratigraphic conditions in the study area: (*a*) map of spatial distribution of DInSAR-derived cumulative settlements at the ground level in the period 2009–2014; (*b*) correlation between the geolithological cross-section across the boreholes B6–B7 (from the portal of the Geological Survey of the Netherland — DINOloket, www.dinoloket.nl) and the cumulative thicknesses of soft soils (organic and clayey), silt and sand vs. DInSAR-derived cumulative settlements along the B6–B7 cross-section. [Colour online.]

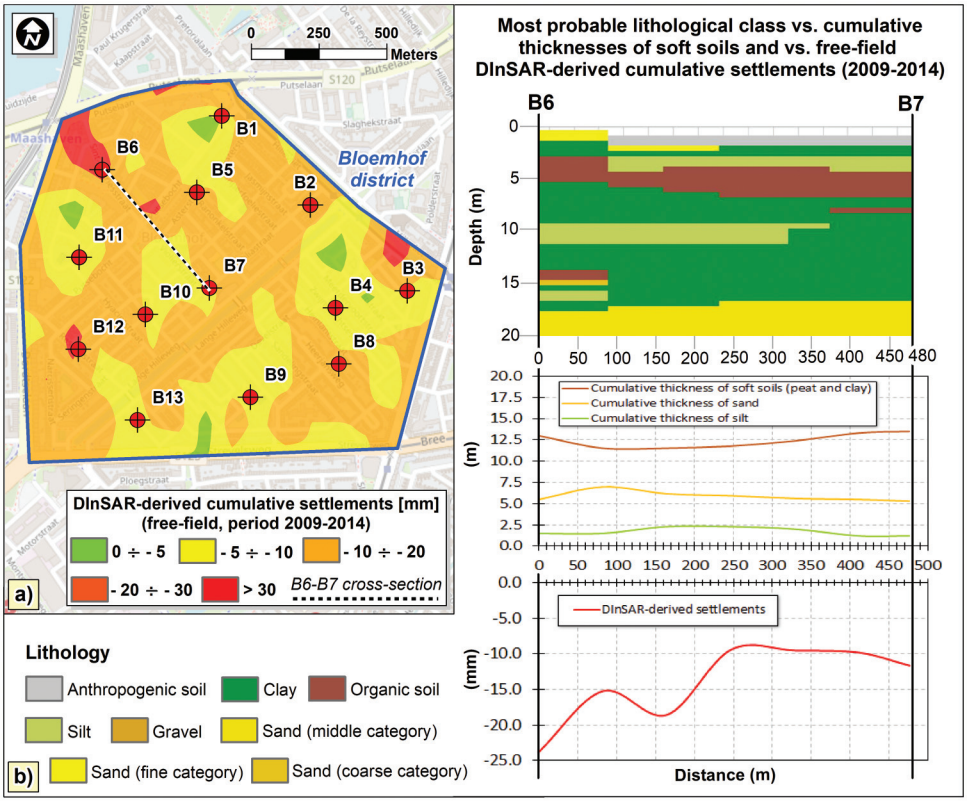

Fig. 6. Plaxis2D-computed cumulative settlements vs. DInSAR-measured cumulative settlements: (*a*) map of coherent DInSAR benchmarks on top of buildings falling within the circular buffer surrounding the 13 considered boreholes; (*b*) results of the quantitative comparison. [Colour online.]

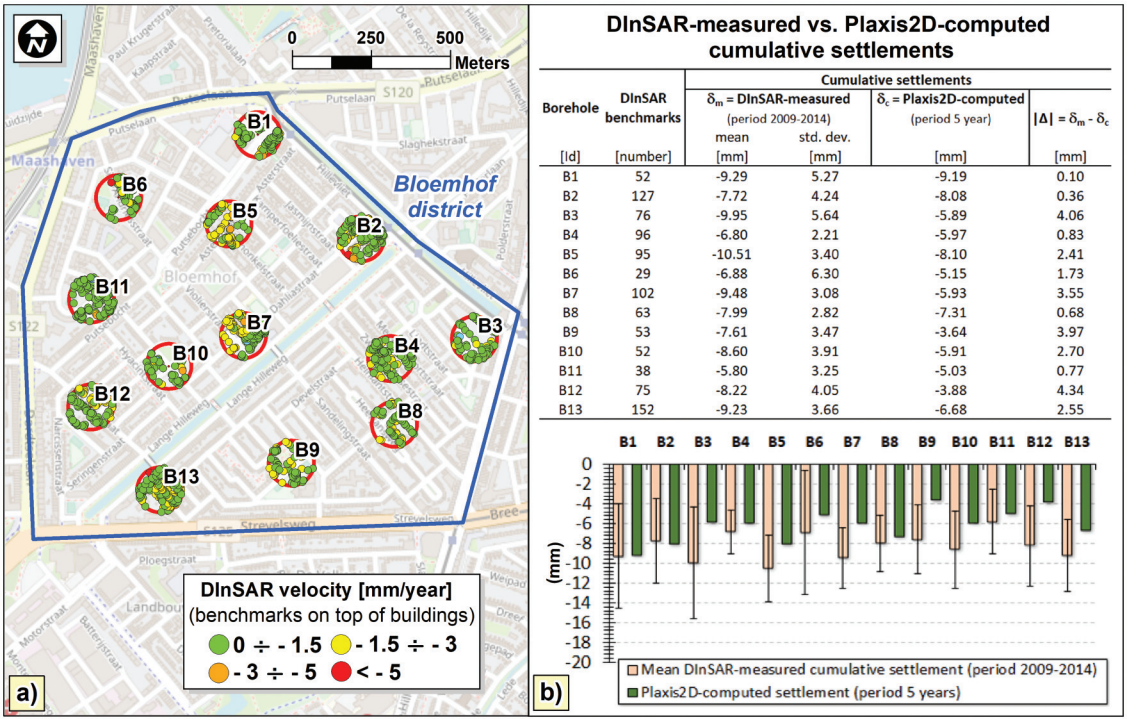

Fig. 7. Different soil scenarios G_i considering (*a*) nearby and (*b*) distant boreholes for the "rapid" and "slow" soil thickness variation in the horizontal direction; (*c*) G_1 — horizontal layers; rapid variation; (*e*) G_2 — inclined layers and (*g*) G_3 — peat inclusion; slow variation; (*d*) G_4 — inclined layers; and (*g*) G_5 — peat inclusion. [Colour online.]

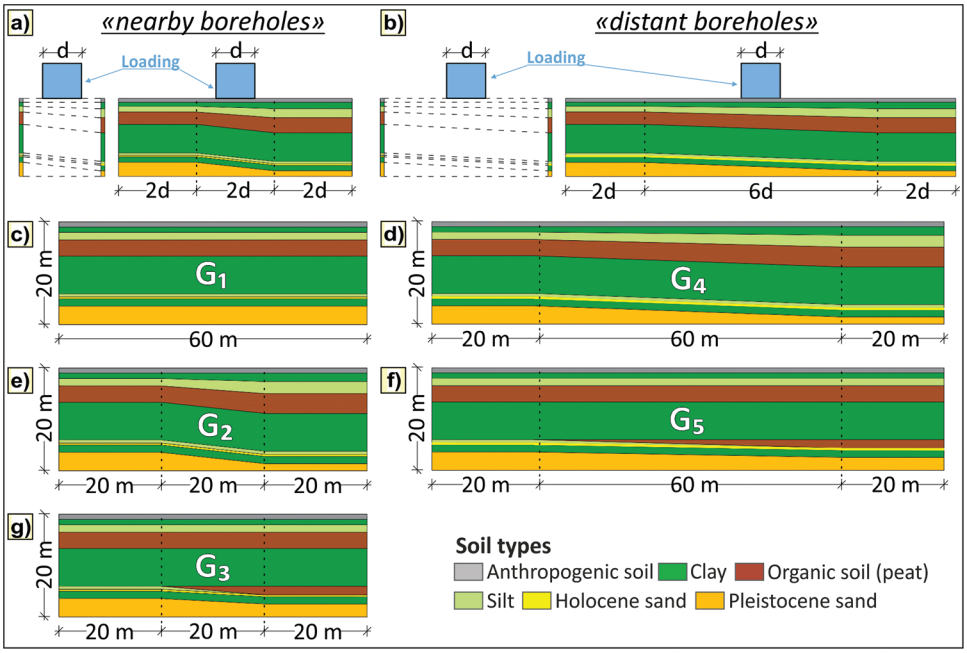

Fig. 8. Five loading conditions derived from (*a*) the selected building. Symmetrical (*b*) L_1 structure and asymmetrical (*c*) L_2, (*d*) L_3, (*e*) L_4, and (*f*) L_5 structures. [Colour online.]

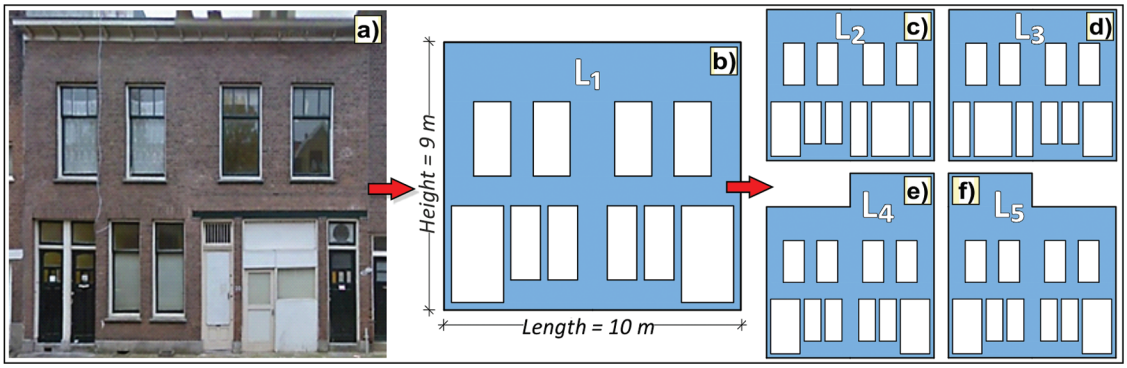

boreholes condition (Fig. 7*b*) represents the typical situation in which a "slow" change in the soil layer (thickness and inclination) occurs between two fixed boreholes that are both located at a distance greater than *d* but not exceeding 3*d* from the middle vertical line of the building; this means that the two considered boreholes are at a distance equal to 6*d* from each other.

Then, based on the above assumptions and considering the length *d* of the building façade to be equal to 10 m (Fig. 8*b*), the G_i soil scenarios shown in Figs. 7*c*–7*g* were obtained. In the first scenario, namely G_1 (Fig 7*c*), horizontal layers were assumed; in particular, the thickness of the soil layers was set equal to the mean values of the soil layers in the analysed boreholes (see Table 2). To define G_2–G_5 scenarios (Figs. 7*d*–*g*), the standard deviation of the soil thickness (shown in Table 2) was summed to the mean soil thickness (peat, clay, and silt were increased, whereas sand was reduced to the same total amount) in the rightmost borehole of the G_1 scenario, thus obtaining two models with inclined layers (G_2 with fast variation and G_4 with slow variation; see Fig. 7*e* and Fig. 7*d*). The G_3 and G_5 scenarios (Figs. 7*g* and 7*f*) represent an inclusion of peat; for this purpose, an additional layer of peat (below the clay layer) with a thickness equal to the value of the standard deviation of the peat layer thickness (see Table 2) was added for the rightmost borehole. This allowed us to define two models with peat inclusion (G_3 with fast variation and G_4 with slow variation; see Fig. 7*g* and Fig. 7*f*). All G_i scenarios reached a depth of 20 m, representing the soil stratigraphy to the depth of the fine to coarse Pleistocene sandy layer of Rotterdam (De Doelder and Hannink 2015) (Fig. 2*b*).

As for the water table levels (H_i; see Table 3), in addition to the case of a constant water table at a depth of 1.50 m (H_1), which was already implemented in the simplified numerical models (i.e., used for an expeditious validation of the assumed soil parameters), two types of time-dependent drawdowns were defined by using the flow function in Plaxis2D. In particular, both a linear drawdown in the time interval of the analysis (30 years) and an immediate drawdown were considered. For each flow function, four water-head variations were assigned, starting from the original level of –1.50 m (–0.25, –0.50, –0.75, –1.00 m), thus obtaining eight water table variations (H_2–H_9 conditions; see Table 3).

Table 3. The drawdown functions assumed for the water level variation in the H_i conditions.

		H_i conditions	
Water level variation (head level) (m)	Water table level (from ground surface) (m)	Linear drawdown	Immediate drawdown
0.00	–1.50	H_1	H_1
–0.25	–1.75	H_2	H_6
–0.50	–2.00	H_3	H_7
–0.75	–2.25	H_4	H_8
–1.00	–2.50	H_5	H_9

Fig. 9. Influence of the mesh coarseness factor (CF) on the computed settlements: an example for $H_1G_2L_5$ model conditions. [Colour online.]

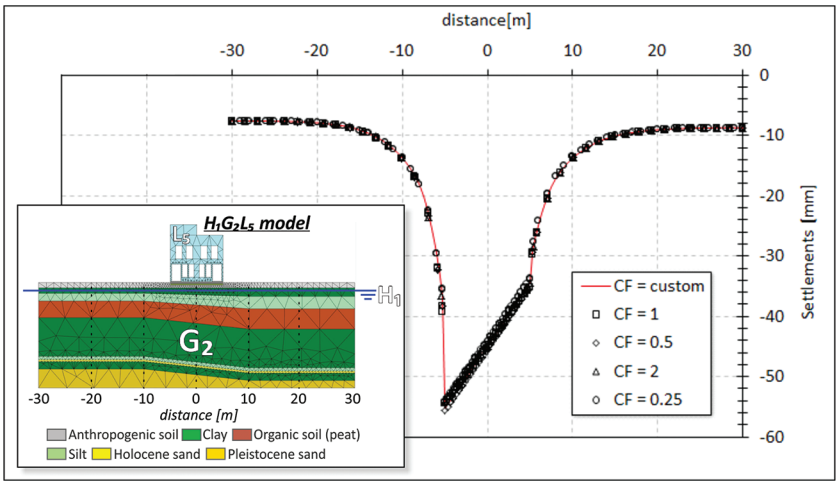

With respect to the building loadings (L_i), Fig. 8*a* shows a typical building in Bloemhof, consisting of a two-unit masonry structure with a two-floored block resting on shallow foundations, whose construction dates back to the 1920s, with an almost symmetrical façade and an average unit weight for masonry assumed equal to 18.00 kN/m^3. Starting from this configuration, five (L_1–L_5) different loading conditions (representative of the building's own weight transmitted to the soil through the foundation system) were considered, taking into account the most common building geometries (i.e., differences in openings or height) and, in turn, loading conditions (resulting in asymmetric loads) retrieved over the district area. Figures 8*b*–8*f* show the considered loading conditions (L_1: symmetrical case; L_2 and L_3: asymmetry in openings; L_4 and L_5: asymmetry in height).

The loading conditions, combined with the geostratigraphic G_i and water table H_i conditions, allowed us to identify the $H_iG_iL_i$ scenarios.

In summary, 225 numerical analyses were performed to implement the typified hydro- (H_1–H_9) geomechanical- (G_1–G_5) loading (L_1–L_5) models. These analyses encompassed a combination of (*i*) nine water level fluctuations (from H_1 to H_9 as reported in Table 3), (*ii*) five stratigraphic conditions representing the most common subsoil scenarios in the study area with fixed geotechnical parameters (from G_1 to G_5, as shown in Fig. 7), and (*iii*) five loading conditions accounting for typical variations in the building shape (from L_1 to L_5 as shown in Fig. 8).

4.3. Phase II: settlement computation and damage assessment

In agreement with other studies addressing the assessment of building damage due to groundwater lowering-induced subsidence in the Netherlands (Costa et al. 2020; Hoogvliet et al. 2012), a time interval of 30 years (10 950 days) was fixed for the numerical simulations.

The defined $H_iG_iL_i$ numerical models were implemented within the PLAXIS2D software in agreement with the assumptions presented in the Methodology section. Furthermore, the analyses were carried out considering the soil – (shallow) foundation interaction. The latter was modelled as interface elements set in PLAXIS2D at the base of the building with a virtual zero thickness and properties related to the soil parameters of the surrounding soil layer. The stiffness of the interface element was computed from the properties of the adjacent soil layer, whereas the strength was manually defined by entering the R_{inter} parameter (representing a reduction factor of the interface mechanical properties with respect to the adjacent soil). Examples of studies available in the literature on shallow foundation systems suggest a common value of R_{inter} equal to 2/3 (Pusadkar and Bhatkar 2013; Sarma 2016) (a value of R_{inter} equal to 1.0 represents a fully bonded interface); therefore this value was chosen for the analyses.

For each $H_iG_iL_i$ combination, the maximum differential settlement was calculated as the difference in the vertical settlement between the side points of the building's footprint. Regarding the deformation boundary conditions, the left and right sides of the modelled soil volume were set as "normally fixed" (i.e., horizontal displacements are fixed), whereas the bottom line was set as "fully fixed" (i.e., both vertical and horizontal displacements are fixed).

Plain strain 15-node triangular elements were used for the discretization, providing 12 integration points. The use of a 15-node triangle leads to slow and time-consuming calculations. Therefore, a preliminary mesh refinement analysis was carried out to

Fig. 10. Settlement troughs computed via numerical simulations in Plaxis2D: an example for loading condition L_5, soil scenario G_2, and H_1–H_9 water level variation. [Colour online.]

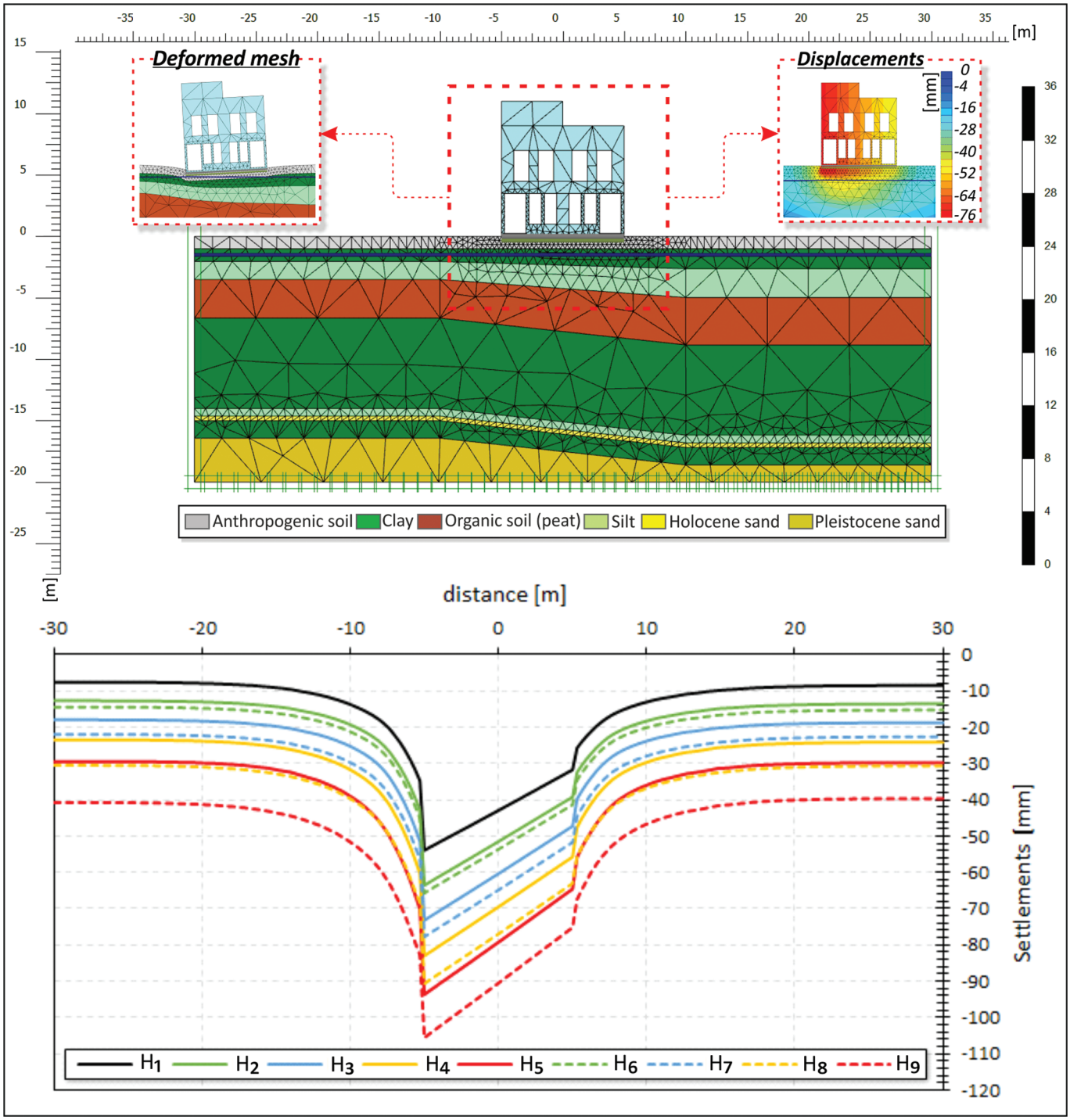

identify the mesh size that allows the optimisation of the required time for running each numerical analysis. In particular, local refinements were obtained by customising the coarseness factor (CF) of the finite elements from a very small coarseness of the subsurface soil close to the load (CF = 0.089) to a higher coarseness (CF = 5.66) in the deeper layers. The influence of the CF on the results in terms of settlement is shown in Fig. 9 with an example of the computed settlement profile for the $H_1G_2L_5$ scenario. Figure 9 shows that the used CF allows the numerical model (namely "custom", red line) to provide results that well approximate (in terms of both the magnitude and the shape of the settlement profiles) those obtained with different CFs. Therefore, the custom CF was proved suitable for the analyses. Furthermore, the choice of a variable CF in the models allowed an optimization of the calculation time. For the same reason, in the numerical analyses, the maximum number of iterations for the convergence criterion for both the deformation and the groundwater flow was fixed at 1×10^3 with a tolerance error of 5×10^{-3}, with each time step consisting of 180 days.

Figure 10 shows the results with reference to loading condition L_5, soil scenario G_2, and groundwater lowering H_1–H_9. Interestingly,

Fig. 11. Computed differential settlements for each typified hydro- (H_i) – geomechanical- (G_i) – loading (L_i) scenario: (*a*) L_1, (*b*) L_2, (*c*) L_3, (*d*) L_4, and (*f*) L_5 loading conditions. [Colour online.]

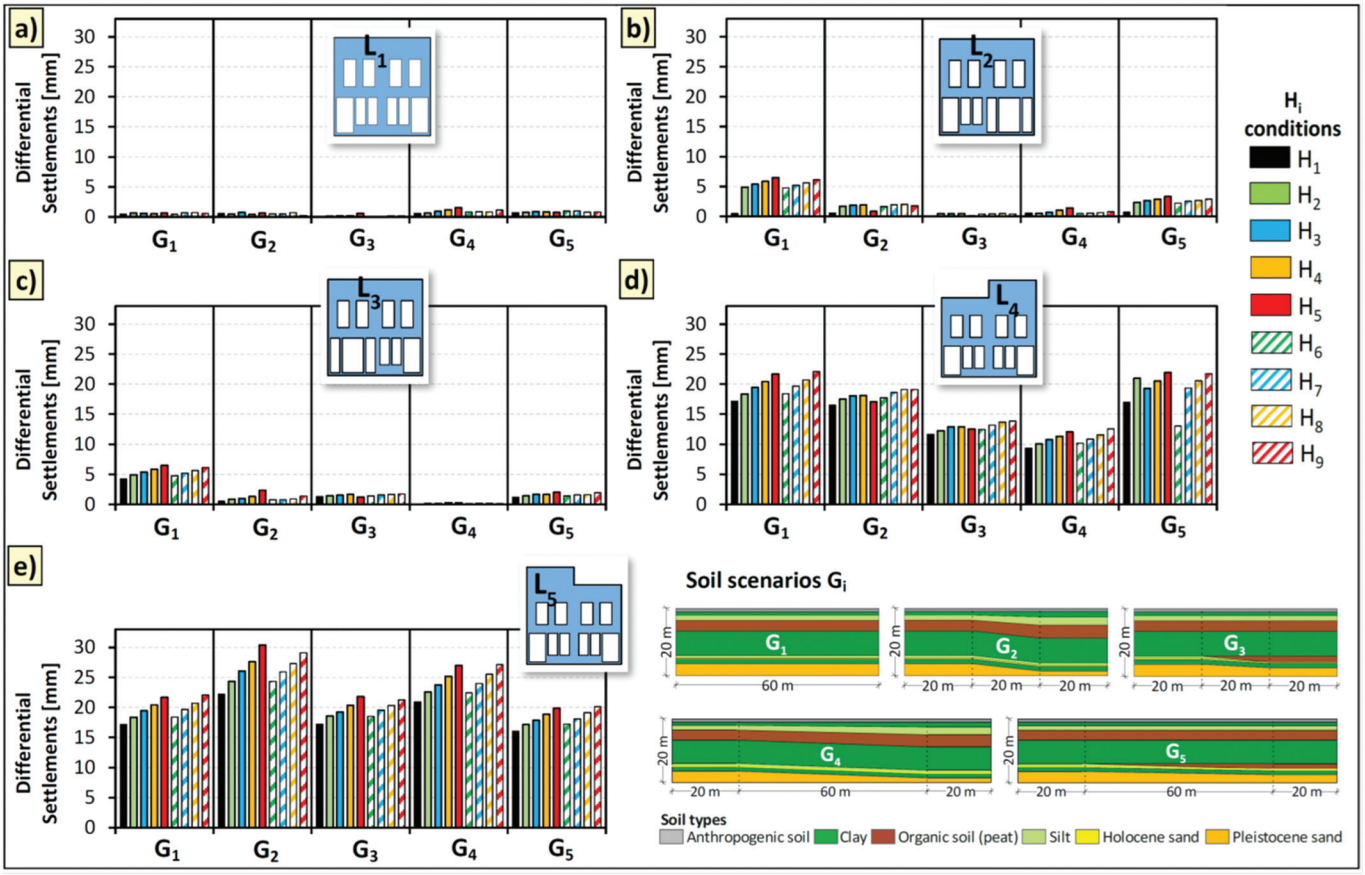

the plots highlight that the highest settlements were recorded for H_6–H_9 scenarios pertaining to immediate drawdown functions (see Table 3).

A comprehensive comparison of the obtained results for the 225 analysed scenarios over 30 years is synthesised in the histograms shown in Fig. 11, in which, for each G_i and L_i condition, the differential settlements measured under the building footprint are plotted according to the different H_i (H_1–H_9) conditions. It can be observed that the differential settlements in a given soil scenario G_i increase with the higher values of the water-head variation for both linear and immediate drawdowns. Moreover, the loading conditions significantly affect the results, as highlighted by the asymmetrical loadings (L_4 and L_5; see Figs. 11*d* and 11*e*) that record higher differential settlement values than the other conditions (L_1–L_3; see Figs. 11*a*, 11*b*, and 11*e*). In the case of the symmetric loading condition L_1 (Fig. 11*a*), the resulting differential settlements showed slight variations in all the soil conditions; however, the highest values were observed in the G_4 scenario. Furthermore, L_2 and L_3 loading conditions (Figs. 11*b* and 11*c*) in the G_i scenarios did not significantly affect the results because they do not add remarkable localised additional stresses (due only to asymmetry in building openings), thus limiting the magnitude of differential settlements. As for loadings L_4 and L_5, two conditions present the highest values of differential settlements (i.e., G_5 and G_2, respectively). This observation suggests that a combination of an asymmetrical structure (here modelled as an asymmetric load) and the heterogeneity of the soil can lead to higher values of differential settlements, thereby confirming the usefulness of assuming inclined soil layers rather than horizontal layers in the half-space, as in the classical approach.

The damage that buildings undergoing the computed differential settlements may experience was assessed using empirical fragility curves for masonry buildings on shallow foundations. Particularly, by entering the curves with the computed differential settlement over 30 years, it was possible to calculate, for each scenario, the probability for the building to reach or exceed a certain damage severity level *Di* (i.e., *D*1 = very slight, *D*2 = slight, *D*3 = moderate damage; see Peduto et al. 2019), which was ranked according to the classification of Burland et al. (1977). Figure 12 shows the results for the L_5 loading condition, which the previous results identified as inducing the highest differential settlements. All different H_i and G_i conditions are accounted for in Fig. 12. In agreement with the previous observations, the highest probabilities of recording the highest damage severity level (*D*3) on the building can be observed in the G_2 (inclined layer with rapid thickness variation) soil scenario. Furthermore, Fig. 12*c* shows lower differential settlements when compared with Fig. 12*b* because the most loaded section of the building and the section of the soil with the highest thickness of peat and clay are on opposite sides. A similar behaviour is displayed in Fig. 12*e*, in which the building load and variability of the soil thickness led to the lowest differential settlements, as if the two conditions compensated for each other.

Interestingly, in Figs. 12*b* and 12*c*, it can be observed that in the case of the highest soil variability (G_2–G_3), an immediate lowering of the water table (H_6–H_9) can bring higher differential settlements than the linear drawdown over time (H_2–H_5) and, in turn, higher potential damage to the buildings.

Finally, the expected damage severity level (*D*) was assessed over 30 years for each building resting on a shallow foundation

Fig. 12. Assessment of the possible damage to buildings undergoing differential settlements using the empirical fragility curves proposed by Peduto et al. (2019). An example for the L_5 loading condition resting on (*a*) G_1, (*b*) G_2, (*c*) G_3, (*d*) G_4, and (*e*) G_5 soil scenarios for the different H_i water level variations. [Colour online.]

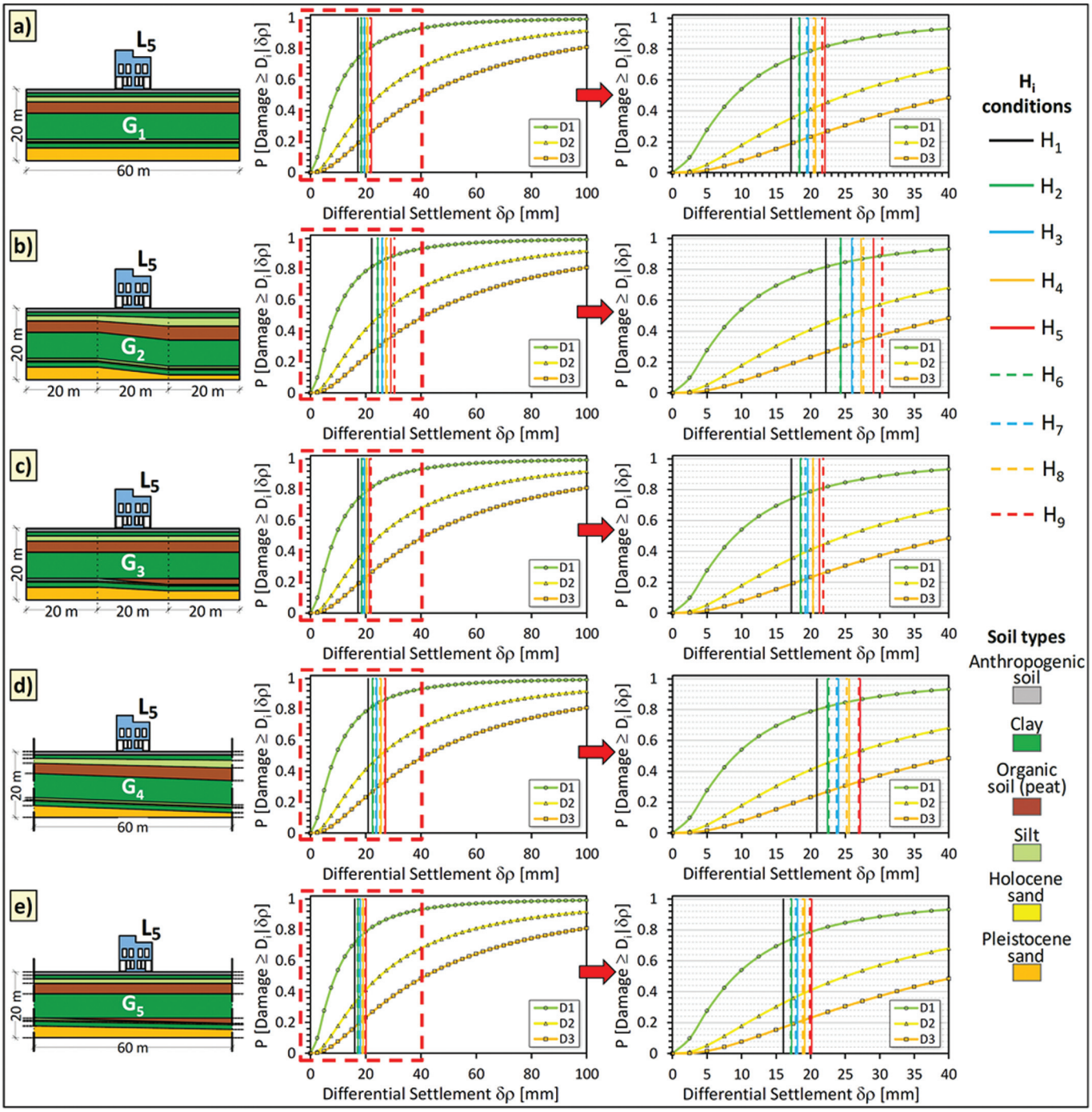

(Fig. 2*d*) in the Bloemhof district. For this purpose, the buildings, considered as undamaged at the initial time of the numerical analysis, were classified according to the defined loading L_1–L_5 (Fig. 13*a*) conditions, and differential settlements were considered as those associated with both a groundwater lowering of 0.25 m (H_2, the most common observed value in the study area) and the worst-case scenario in the considered soil assets (G_2). The D level was derived considering the mean expected level of damage severity (ED) by adapting eq. 1 proposed by Pitilakis and Fotopoulou (2015):

$$\text{ED(SRI)} = \sum_{i=0}^{1} p_i d_i \quad (1)$$

where ED can be estimated as the weighted sum of the discrete damage probability (p_i) associated with the occurrence of the ith expected damage severity level (D_i), which can be retrieved from the fragility curves in correspondence of the computed value of the selected SRI parameter (i.e., expected differential settlement over 30 years) multiplied by a numerical index (d_i) whose value

Fig. 13. Map of masonry buildings with shallow foundations in the Bloemhof district distinguished according to (*a*) the defined (L_1–L_5) loading conditions and (*b*) the expected damage severity level over 30 years. [Colour online.]

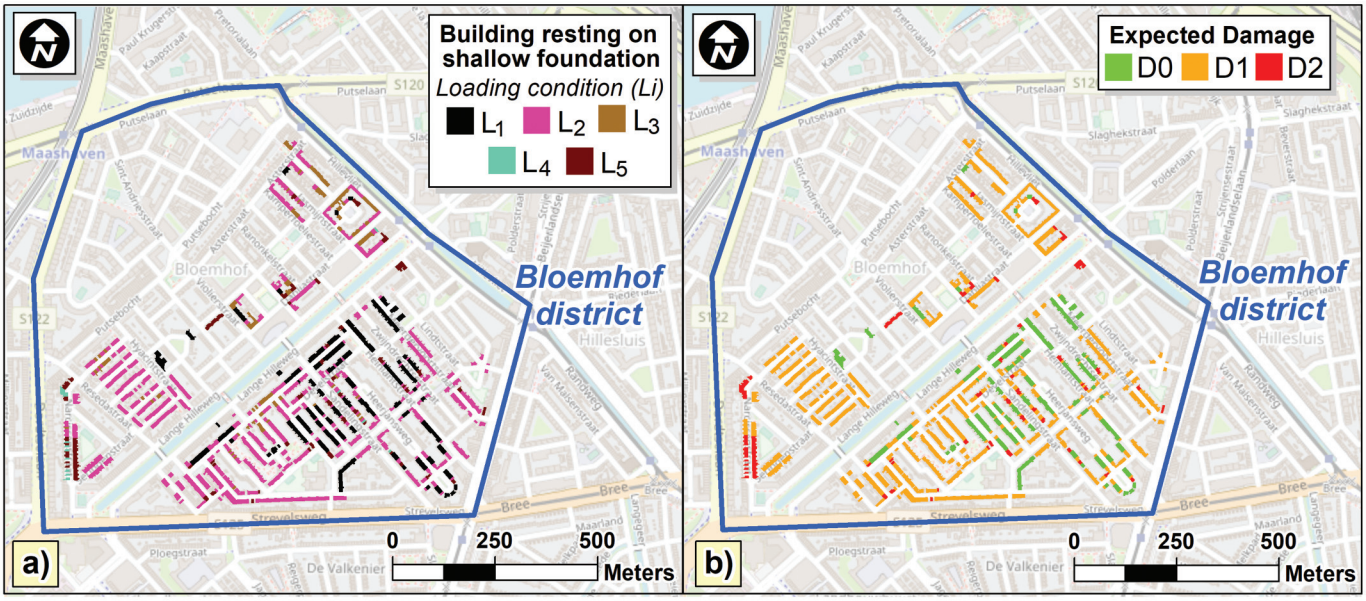

changes according to the considered expected *Di* (e.g., assumed equal to 0.20, 0.40, 0.60, 0.80, and 1.0 for, respectively, *D*1, *D*2, *D*3, *D*4, and *D*5 of Burland et al.'s (1977) classification). ED ranges between zero and 1. The expected damage (*D*) was assumed equal to *D*0 for ED = 0, *D*1 for 0 < ED ≤ 0.20, *D*2 for 0.20 <ED ≤ 0.40, *D*3 for 0.40 <ED ≤ 0.60, *D*4 for 0.60 <ED ≤ 0.80, and *D*5 for 0.80 < ED ≤ 1.

For the selected combination, the results (Fig. 13*b*) show that within the next 30 years, for the total number of 1398 buildings on shallow foundations, 375 were not expected to show any significant damage (*D*0), 896 buildings were estimated to show very slight aesthetic damage (*D*1), and 127 buildings may present slight damage (*D*2). The relatively small *D* levels are in agreement with the relatively low values of displacements measured on top of buildings in the study area (Fig. 3*d*), and the *D* computed in these analyses is underestimated because the current maintenance state of buildings was not taken into account.

5. Discussion and conclusion

This study presented an innovative approach that, based on a combination of information on the subsoil settings, groundwater regime, and building loading conditions, set up 225 simplified HGL scenarios to represent typical geotechnical conditions of buildings in a subsiding district. These models were then implemented in numerical simulations for settlement computation and building damage assessment. The availability of a well-organised database of subsoil and groundwater in the Netherlands, in combination with extensive DInSAR-derived settlement measurements, provided a sound base for the analyses carried out in the chosen district.

The analyses allowed us to investigate the role of three main factors (i.e., soil heterogeneity, loading conditions, and groundwater variations) on both the magnitude and spatial distribution of settlements in the study area, thus representing a step forward in the evaluation of the effects of soil variability in the analyses and predictions of settlement-induced damage to buildings.

The obtained results show that, although the lowering of the water table in the study area is considered the main triggering factor of subsidence, both the loading conditions and soil variability are capable of amplifying the differential settlements and, in turn, the damage suffered by the buildings.

The results of the numerical simulations were also used in combination with fragility curves to assess the building damage. This was possible because of the availability of empirical fragility curves, which were specifically derived for buildings with similar structural–foundation typology and in the same hydro-geolithological context. Obviously, the proposed approach is more reliable in areas where settlement-induced damage to buildings is not associated with local geotechnical–structural weakness but involves large areas under similar conditions (as in the Netherlands). An improvement of the presented analyses should deal with advanced geostatistical analyses to account for the uncertainties related to the synergistic use of multi-source datasets to infer the reliability of risk analyses. Furthermore, the current state of building maintenance should also be accounted for; this was not possible in this study because the available fragility curves used for damage forecasting did not include this information.

For the selected district, the displacement magnitudes measured on top of the buildings were rather limited; notwithstanding, in case of a lack of countermeasures, with the passing of time an increase of differential displacements is likely to bring more severe damage.

Importantly, a lack of information can be a limitation for this type of analysis. Indeed, the proposed procedure was tested under very favourable conditions (e.g., a flat area, reliable subsoil–groundwater data, very-high-resolution DInSAR data, buildings with homogeneous characteristics in the chosen area, and rich datasets); consequently, the quality of the available data influenced the achievement of the obtained results. Moreover, the application of the procedure over wider areas (e.g., on a city, region, country scale) may require time-consuming data collection, where available, as well as more demanding efforts to identify the considered "typified" scenarios.

It is necessary to emphasise that these analyses should be considered propaedeutic for detailed investigations of single buildings for which the highest differential settlements were computed and the most severe expected damage was assessed. For these identified cases, building damage analysis requires a thorough modelling of the soil–foundation–superstructure interaction, which in the presented approach was simplified because of the extent of the study area. In addition, investigating the subsoil system heterogeneity would require (*i*) an insight into the spatial–time dependency of

the groundwater regime (e.g., the implemented drawdown functions represent a uniform lowering of the phreatic water table, although fluctuations and differential lowering of the water table are observable in the measurements) and (*ii*) a detailed analysis of the soil property spatial variability.

Finally, taking into account that in the Netherlands, such phenomena are widespread and both expensive investigations and maintenance works are carried out yearly, the adoption of wide-area approaches could allow the expeditious modelling of the building performance at the municipal–neighbourhood scale. This could represent an efficient way for geotechnical engineers to provide institutions, territorial agencies, and private owners with an overview of subsidence-related criticalities and to promote specific interventions from the perspective of sustainable subsidence risk mitigation.

Acknowledgements

This work was supported by two ERASMUS+ for Traineeship Agreements between the University of Salerno (Italy) and Deltares (the Netherlands) and between the University of Salerno (Italy) and SkyGeo Netherlands B.V. The authors gratefully acknowledge Sky-Geo Netherlands B.V for supplying the DInSAR data.

References

Abdollahi, S., Pourghasemi, H.R., Ghanbarian, G.A., and Safaeian, R. 2019. Prioritization of effective factors in the occurrence of land subsidence and its susceptibility mapping using an SVM model and their different kernel functions. Bulletin of Engineering Geology and the Environment, **78**(6): 4017–4034. doi:10.1007/s10064-018-1403-6.

Arangio, S., Calò, F., Di Mauro, M., Bonano, M., Marsella, M., and Manunta, M. 2014. An application of the SBAS-DInSAR technique for the assessment of structural damage in the city of Rome. Structure and Infrastructure Engineering, **10**(11): 1469–1483. doi:10.1080/15732479.2013.833949.

Bischoff, C.A., Ferretti, A., Novali, F., Uttini, A., Giannico, C., and Meloni, F. 2020. Nationwide deformation monitoring with SqueeSAR® using Sentinel-1 data. Proceedings of the International Association of Hydrological Sciences, **382**: 31–37. doi:10.5194/piahs-382-31-2020.

Bjerrum, L. 1963. Allowable settlement of structures. *In* Proceedings of European Conference on Soil Mechanics and Foundation Engineering, Weisbaden, Germany, 15–18 October 1963. Vol. 3. pp. 135–137.

Boscardin, M.D., and Cording, E.J. 1989. Building response to excavation-induced settlement. Journal of Geotechnical Engineering, ASCE, **115**(1): 1–21. doi:10.1061/(ASCE)0733-9410(1989)115:1(1).

Breysse, D., Niandou, H., Elachachi, S., and Houy, L. 2005. A generic approach to soil–structure interaction considering the effects of soil heterogeneity. Géotechnique, **55**(2): 143–150. doi:10.1680/geot.2005.55.2.143.

Bucx, T.H.M., Van Ruiten, C.J.M., Erkens, G., and De Lange, G. 2015. An integrated assessment framework for land subsidence in delta cities. Proceedings of the International Association of Hydrological Sciences, **372**: 485–491. doi:10.5194/piahs-372-485-2015.

Burland, J.B., and Wroth, C.P. 1974. Settlements of buildings and associated damage. *In* Proceedings of the Conference on Settlement of Structures. Pentech Press, London, UK. pp 611–654.

Burland, J.B., Broms, B.B., and De Mello, V.F. 1977. Behaviour of foundations and structures. SOA report. *In* Proceedings of the 9th International Conference on Soil Mechanics and Foundation Engineering, Tokyo, Japan. Vol. 2. pp. 495–546.

Chang, L., Dollevoet, R.P., and Hanssen, R.F. 2017. Nationwide railway monitoring using satellite SAR interferometry. IEEE Journal of Selected Topics in Applied Earth Observations and Remote Sensing, **10**(2): 596–604. doi:10.1109/JSTARS.2016.2584783.

Costa, A.L., Kok, S., and Korff, M. 2020. Systematic assessment of damage to buildings due to groundwater lowering-induced subsidence: methodology for large scale application in the Netherlands. Proceedings of the International Association of Hydrological Sciences, **382**: 577–582. doi:10.5194/piahs-382-577-2020.

De Doelder, B., and Hannink, G. 2015. Risk management of groundwater during the reconstruction of the Rotterdam central area. *In* Geotechnical Safety and Risk V. IOS Press. pp. 583–589.

de Sanctis, L., and Mandolini, A. 2006. Bearing capacity of piled rafts on soft clay soils. Journal of Geotechnical and Geoenvironmental Engineering, ASCE, **132**(12): 1600–1610. doi:10.1061/(ASCE)1090-0241(2006)132:12(1600).

Dufour, F.C. 2000. Groundwater in the Netherlands — Facts and figures [online]. Netherlands Institute of Applied Geoscience TNO — National Geological Survey, Delft/Utrecht. Available from http://resolver.tudelft.nl/uuid:ad3ca585-1991-450b-8b2f-48ef5f1f46df.

Elkateb, T., Chalaturnyk, R., and Robertson, P.K. 2003. An overview of soil heterogeneity: quantification and implications on geotechnical field problems. Canadian Geotechnical Journal, **40**(1): 1–15. doi:10.1139/t02-090.

Erkens, G., Bucx, T., Dam, R., De Lange, G., and Lambert, J. 2015. Sinking coastal cities. Proceedings of the International Association of Hydrological Sciences, **372**: 189–198. doi:10.5194/piahs-372-189-2015.

Esri Nederland – BAG 3D. 2020. BAG 3D – Nederland [online]. Available from https://www.arcgis.com/home/item.html?id=abd5e3c4b173417f8c14f1283dee33c6 [accessed September 2020].

Ezquerro, P., Guardiola-Albert, C., Herrera, G., Fernández-Merodo, J.A., Béjar-Pizarro, M., and Bonì, R. 2017. Groundwater and subsidence modeling combining geological and multi-satellite SAR data over the alto guadalentín aquifer (SE Spain). Geofluids, **2017**: 1359325. doi:10.1155/2017/1359325.

Ferlisi, S., Nicodemo, G., Peduto, D., Negulescu, C., and Grandjean, G. 2020. Deterministic and probabilistic analyses of the 3D response of masonry buildings to imposed settlement troughs. Georisk, **14**(4): 260–279. doi:10.1080/17499518.2019.1658880.

Ferlisi, S., Marchese, A., and Peduto, D. 2021. Quantitative analysis of the risk to road networks exposed to slow-moving landslides: a case study in the Campania region (southern Italy). Landslides, **18**: 303–319. doi:10.1007/s10346-020-01482-8.

Fernández-Torres, E., Cabral-Cano, E., Solano-Rojas, D., Havazli, E., and Salazar-Tlaczani, L. 2020. Land Subsidence risk maps and InSAR based angular distortion structural vulnerability assessment: an example in Mexico City. Proceedings of the International Association of Hydrological Sciences, **382**: 583–587. doi:10.5194/piahs-382-583-2020.

Frantziskonis, G., and Breysse, D. 2003. Influence of soil variability on differential settlements of structures. Computers and Geotechnics, **30**(3): 217–230. doi:10.1016/S0266-352X(02)00062-9.

Funderingskaart. 2019. Funderingstypekaart Rotterdam [online]. Available from https://www.arcgis.com/apps/MapSeries/index.html?appid=e0ff1f373bca4574a751529c7bc536d7 [accessed September 2020].

Gemeente Rotterdam. 2020. Gis Rotterdam [online]. Available from https://www.gis.rotterdam.nl/gisweb2/default.aspx [accessed September 2020].

Ghodsvali, M. 2018. 3D modelling of underground space for urban planning and management-providing basic planning insight. M.Sc. thesis, Faculty of Geo-Information Science and Earth Observation, University of Twente, the Netherlands.

Giardina, G., Milillo, P., DeJong, M.J., Perissin, D., and Milillo, G. 2019. Evaluation of InSAR monitoring data for post-tunnelling settlement damage assessment. Structural Control and Health Monitoring, **26**(2): e2285. doi:10.1002/stc.2285.

Guzy, A., and Malinowska, A.A. 2020. State of the art and recent advancements in the modelling of land subsidence induced by groundwater withdrawal. Water, **12**(7): 2051. doi:10.3390/w12072051.

Hanssen, F.R. 2003. Subsidence monitoring using contiguous and PSINSAR: quality assessment based on precision and reliability. *In* Proceeding of the 11th FIG Symposium on Deformation Measurements, Santorini, Greece, 25–28 May 2003. pp. 1–8.

Herrera, G., Fernández, J.A., Tomás, R., Cooksley, G., and Mulas, J. 2009. Advanced interpretation of subsidence in Murcia (SE Spain) using A-DInSAR data-modelling and validation. Natural Hazards and Earth System Sciences, **9**(3): 647–661. doi:10.5194/nhess-9-647-2009.

Herrera-García, G., Ezquerro, P., Tomás, R., Béjar-Pizarro, M., López-Vinielles, J., Rossi, M., et al. 2021. Mapping the global threat of land subsidence. Science, **371**(6524): 34–36. doi:10.1126/science.abb8549.

Hoogvliet, M., Buma, J., Oostrom, N. van, Brolsma, R, Filatova, T., and Verheijen, J., 2012. Schades Door Watertekorten En — Overschotten in Stedelijk Gebied [online]. Deltares Report 1205463-000. Deltares, Delft, the Netherlands. Available from http://publications.deltares.nl/1205463_000a.pdf [accessed September 2020].

Hooimeijer, F.L., Lafleur, F., and Trinh, T.T. 2017. Drawing the subsurface: an integrative design approach. Procedia Engineering, **209**: 61–74. doi:10.1016/j.proeng.2017.11.131.

Koster, K., Stafleu, J., and Stouthamer, E. 2018. Differential subsidence in the urbanised coastal-deltaic plain of the Netherlands. Netherlands Journal of Geosciences, **97**(4): 215–227. doi:10.1017/njg.2018.11.

Lee, S., and Park, I. 2013. Application of decision tree model for the ground subsidence hazard mapping near abandoned underground coal mines. Journal of Environmental Management, **127**: 166–176. doi:10.1016/j.jenvman.2013.04.010.

Leusink, E. 2018. Naar een kosteneffectieve aanpak van klimaatadaptatie in Nederland [online]. Available from https://ruimtelijkeadaptatie.nl/publish/pages/170697/pr3936_10_hoofdrapport_20190424_definitief.pdf [accessed September 2020].

Mahmoudpour, M., Khamehchiyan, M., Nikudel, M.R., and Ghassemi, M.R. 2016. Numerical simulation and prediction of regional land subsidence caused by groundwater exploitation in the southwest plain of Tehran, Iran. Engineering Geology, **201**: 6–28. doi:10.1016/j.enggeo.2015.12.004.

Marache, A., Dubost, J., Breysse, D., Denis, A., and Dominique, S. 2009. Understanding subsurface geological and geotechnical complexity at various scales in urban soils using a 3D model. Georisk, **3**(4): 192–205. doi:10.1080/17499510802711994.

Mas-Pla, J., Rodríguez-Florit, A., Zamorano, M., Roqué, C., Menció, A., and Brusi, D. 2013. Anticipating the effects of groundwater withdrawal on seawater intrusion

and soil settlement in urban coastal areas. Hydrological Processes, **27**(16): 2352–2366. doi:10.1002/hyp.9377.

Modoni, G., Darini, G., Spacagna, R.L., Saroli, M., Russo, G., and Croce, P. 2013. Spatial analysis of land subsidence induced by groundwater withdrawal. Engineering Geology, **167**: 59–71. doi:10.1016/j.enggeo.2013.10.014.

Nappo, N., Peduto, D., Mavrouli, O., van Westen, C.J., and Gullà, G. 2019. Slow-moving landslides interacting with the road network: analysis of damage using ancillary data, in situ surveys and multi-source monitoring data. Engineering Geology, **260**: 105244. doi:10.1016/j.enggeo.2019.105244.

NEN 9997-1+C2. 2017. Geotechnical design of structures — Part 1: General rules. ICS Code 93.020.

NPR 9998. 2020. Assessment of structural safety of buildings in case of erection, reconstruction and disapproval — Induced earthquakes — Basis of design, actions and resistances.

Nicodemo, G., Peduto, D., Ferlisi, S., and Maccabiani, J. 2017. Investigating building settlements via very high resolution SAR sensors. *In* Life-Cycle of Engineering Systems: Emphasis on Sustainable Civil Infrastructure. *Edited by* J. Bakker, D.M. Frangopol, and K. van Breugel. Taylor & Francis Group, London, UK. pp. 2256–2263.

Nicodemo, G., Ferlisi, S., Peduto, D., Aceto, L., and Gullà, G. 2020*a*. Damage to masonry buildings interacting with slow-moving landslides: a numerical analysis. *In* Geotechnical Research for Land Protection and Development. Lecture Notes in Civil Engineering. Vol. 40. *Edited by* F. Calvetti, F. Cotecchia, A. Galli, and C. Jommi. Springer, Cham. pp. 52–61. doi:10.1007/978-3-030-21359-6_6.

Nicodemo, G., Peduto, D., and Ferlisi, S. 2020*b*. Building damage assessment and settlement monitoring in subsidence-affected urban areas: case study in the Netherlands. Proceedings of the International Association of Hydrological Sciences, **382**: 651–656. doi:10.5194/piahs-382-651-2020.

Nicodemo, G., Peduto, D., Korff, M., and Ferlisi, S. 2020*c*. Multi-parameter probabilistic vulnerability analysis of settlement-affected masonry buildings with shallow/piled foundations in soft soils: case studies in the Netherlands. *In* Geotechnical Research for Land Protection and Development Lecture Notes in Civil Engineering. Vol. 40. *Edited by* F. Calvetti, F. Cotecchia, A. Galli, and C. Jommi. Springer, Cham. pp. 42–51. doi:10.1007/978-3-030-21359-6_5.

Peduto, D., Huber, M., Speranza, G., van Ruijven, J., and Cascini, L. 2017*a*. DInSAR data assimilation for settlement prediction: case study of a railway embankment in the Netherlands. Canadian Geotechnical Journal, **54**(4): 502–517. doi:10.1139/cgj-2016-0425.

Peduto, D., Nicodemo, G., Maccabiani, J., and Ferlisi, S. 2017*b*. Multi-scale analysis of settlement-induced building damage using damage surveys and DInSAR data: a case study in the Netherlands. Engineering Geology, **218**: 117–133. doi:10.1016/j.enggeo.2016.12.018.

Peduto, D., Elia, F., and Montuori, R. 2018. Probabilistic analysis of settlement-induced damage to bridges in the city of Amsterdam (the Netherlands). Transportation Geotechnics, **14**: 169–182. doi:10.1016/j.trgeo.2018.01.002.

Peduto, D., Korff, M., Nicodemo, G., Marchese, A., and Ferlisi, S. 2019. Empirical fragility curves for settlement-affected buildings: analysis of different intensity parameters for seven hundred masonry buildings in the Netherlands. Soils and Foundations, **59**(2): 380–397. doi:10.1016/j.sandf.2018.12.009.

Peduto, D., Giangreco, C., and Venmans, A.A.M. 2020. Differential settlements affecting transition zones between bridges and road embankments on soft soils: numerical analysis of maintenance scenarios by multi-source monitoring data assimilation. Transportation Geotechnics, **24**: 100369. doi:10.1016/j.trgeo.2020.100369.

Piciullo, L., Ritter, S., Lysdahl, A.O.K., Langford, J., and Nadim, F. 2021. Assessment of building damage due to excavation-induced displacements: the GIBV method. Tunnelling and Underground Space Technology, **108**: 103673. doi:10.1016/j.tust.2020.103673.

Pitilakis, K.D., and Fotopoulou, S.D. 2015. Vulnerability assessment of buildings exposed to coseismic permanent slope displacements. *In* Geotechnical Engineering for Infrastructure and Development. *Edited by* M.G. Winter, D.M. Smith, P.J.L. Eldred, and D.G. Toll. ICE Publishing, London, UK. pp. 151–173.

Polshin, D.E., and Tokar, R.A. 1957. Maximum allowable non-uniform settlement of structures. *In* Proceedings of the 4th International Conference on Soil Mechanics and Foundation Engineering, London, UK, 12–24 August 1957. Vol. 1. Butterworth's, London, UK. pp. 402–405.

Popescu, R., Deodatis, G., and Nobahar, A. 2005. Effects of random heterogeneity of soil properties on bearing capacity. Probabilistic Engineering Mechanics, **20**(4): 324–341. doi:10.1016/j.probengmech.2005.06.003.

Pratesi, F., Tapete, D., Terenzi, G., Del Ventisette, C., and Moretti, S. 2015. Rating health and stability of engineering structures via classification indexes of InSAR persistent scatterers. International Journal of Applied Earth Observation and Geoinformation, **40**: 81–90. doi:10.1016/j.jag.2015.04.012.

Pusadkar, S.S., and Bhatkar, T. 2013. Behaviour of raft foundation with vertical skirt using plaxis 2D. International Journal of Engineering Research and Development, **7**(6): 20–24.

Randolph, M.F. 1994. Design methods for pile groups and piled rafts. *In* Proceeding of the 13th International Conference on Soil Mechanics and Foundation Engineering, New Delhi, India, 5–10 January 1994. pp. 61–82.

Raspini, F., Bianchini, S., Moretti, S., Loupasakis, C., Rozos, D., Duro, J., and Garcia, M. 2016. Advanced interpretation of interferometric SAR data to detect, monitor and model ground subsidence: outcomes from the ESA-GMES Terrafirma project. Natural Hazards, **83**(1): 155–181. doi:10.1007/s11069-016-2341-x.

Rosi, A., Tofani, V., Agostini, A., Tanteri, L., Tacconi Stefanelli, C., Catani, F., and Casagli, N. 2016. Subsidence mapping at regional scale using persistent scatters interferometry (PSI): The case of Tuscany region (Italy). International Journal of Applied Earth Observation and Geoinformation, **52**: 328–337. doi:10.1016/j.jag.2016.07.003.

Russo, G., and Viggiani, C. 1998. Factors controlling soil-structure interaction for piled rafts. *In* Proceedings of the International Conference on Soil-Structure-Interaction in Urban Civil Engineering. Darmstadt Geotechnics, Darmstadt University of Technology. Vol. 4. pp. 297–322.

Saeidi, A., Deck, O., and Verdel, T. 2012. Development of building vulnerability functions in subsidence regions from analytical methods. Géotechnique, **62**(2): 107–120. doi:10.1680/geot.9.P.028.

Sarma, K. 2016. Load-displacement behaviour of skirted raft foundations on sand using PLAXIS 2D. International Journal of Advanced Engineering Research and Science, **3**(4): 258871.

Shahriar, M.A., Sivakugan, N., Urquhart, A., Tapiolas, M., and Das, B.M. 2013. A study on the influence of ground water level on foundation settlement in cohesionless soil. *In* Processing of the 18th International Conference on Soil Mechanics and Geotechnical Engineering, Paris, France, 2–6 September 2013. pp. 216–229.

Shen, S.L., and Xu, Y.S. 2011. Numerical evaluation of land subsidence induced by groundwater pumping in Shanghai. Canadian Geotechnical Journal, **48**(9): 1378–1392. doi:10.1139/t11-049.

Skempton, A.W., and MacDonald, D.H. 1956. The allowable settlements of buildings. Proceedings of the Institution of Civil Engineers, **5**(6): 727–768. doi:10.1680/ipeds.1956.12202.

Stafleu, J., Maljers, D., Gunnink, J.L., Menkovic, A., and Busschers, F.S. 2011. 3D modelling of the shallow subsurface of Zeeland, the Netherlands. Netherlands Journal of Geosciences – Geologie en Mijnbouw, **90**(4): 293–310. doi:10.1017/S0016774600000597.

van den Born, G.J., Kragt, F., Henkens, D., Rijken, B., van Bemmel, B., van der Sluis, S., et al. 2016. Dalende bodems, stijgende kosten: mogelijke maatregelen tegen veenbodemdaling in het landelijk en stedelijk gebied: beleidsstudie (PBL-publicatie; No. 1064) [online]. Planbureau voor de Leefomgeving. Available from https://edepot.wur.nl/399337 [accessed September 2020].

van der Meulen, M.J., Doornenbal, J.C., Gunnink, J.L., Stafleu, J., Schokker, J., Vernes, R.W., et al. 2013. 3D geology in a 2D country: perspectives for geological surveying in the Netherlands. Netherlands Journal of Geosciences – Geologie en Mijnbouw, **92**(4): 217–241. doi:10.1017/S0016774600000184.

Wu, H.N., Shen, S.L., Chen, R.P., and Zhou, A. 2020*a*. Three-dimensional numerical modelling on localised leakage in segmental lining of shield tunnels. Computers and Geotechnics, **122**: 103549. doi:10.1016/j.compgeo.2020.103549.

Wu, Y.X., Shen, S.L., Lyu, H.M., and Zhou, A. 2020*b*. Analyses of leakage effect of waterproof curtain during excavation dewatering. Journal of Hydrology, **583**: 124582. doi:10.1016/j.jhydrol.2020.124582.

Zhang, L.M., and Ng, A.M.Y. 2005. Probabilistic limiting tolerable displacements for serviceability limit state design of foundations. Géotechnique, **55**(2): 151–161. doi:10.1680/geot.2005.55.2.151.